JOURNAL OF MATERIALS SCIENCE 23 (1988) 2975–2982

Age-hardening and the associated phase transformation in an Au–55.2 at % Cu–17.4 at % Ag ternary alloy

MASAHARU NAKAGAWA, KATSUHIRO YASUDA
Department of Dental Materials Science, Nagasaki University School of Dentistry, Nagasaki 852, Japan

To develop a low gold content dental alloy, age-hardening characteristics in an Au–55.2 at % Cu–17.4 at % Ag alloy were studied by means of hardness, electron microscopy and X-ray diffraction examination. Three distinct age-hardening behaviours depending on temperature were found in the alloy, i.e. (i) a dual mechanism of spinodal decomposition and Cu_3Au ordering below 673 K, (ii) a single mechanism of spinodal decomposition at 693 K, and (iii) a single mechanism of nucleation and growth of silver-rich precipitate at 773 K. A marked over-ageing was observed by lengthy ageing over the whole range of temperature. The long-period superstructure of Cu_3Au(II) was found only in the grain boundary product at temperatures between 623 and 633 K.

1. Introduction

It has been well known that the ternary system of gold–copper–silver shows a conspicuous age-hardening in some composition regions characterized by ordering and/or two-phase decomposition. It is supposed that the age-hardening characteristics of these alloys are affected by the relative composition of constituents, especially by the atomic ratio of gold and copper to form the Au–Cu ordered phase. Because the tendency for two-phase decomposition may increase markedly as the gold content in the alloys decreases, the effect of the Au–Cu ordered phase on the hardening may degenerate or be suppressed.

The effect on the age-hardening mechanism of the variation of gold content in the ternary alloys 18 carat, 16 carat and 14 carat gold alloys, for which the atomic ratio of copper to silver remained 76 to 24, have been studied by means of selected-area electron diffraction (SAED) and transmission electron microscopy (TEM) in addition to X-ray diffraction, electrical resistivity and hardness measurements [1–4]. Recently, a coherent phase diagram of the $Au_x(Ag_{0.24}Cu_{0.76})_{1-x}$ section in the gold–copper–silver ternary system was determined by means of TEM and SAED techniques by the present authors [5]. In the course of the study concerning the coherent phase diagram, we found a significant age-hardening in a low gold content alloy caused by a dual mechanism of $L1_2$-type Cu_3Au ordering and two-phase decomposition.

The present paper, therefore, gives an account of the age-hardening and the associated phase transformation in a 12 carat gold–copper–silver ternary alloy in which the atomic ratio of copper to silver was also 76 to 24. This may afford appropriate guidance for the development of low gold content alloys in which the age-hardenability is equal to those found in high gold content dental alloys.

2. Experimental procedure

An alloy which contained 27.4 at % Au, 55.2 at % Cu and 17.4 at % Ag was prepared by vacuum-melting in a high-frequency induction furnace. The alloying constituents used were 99.99% purity materials. To ensure uniformity of composition, the alloy ingot was swaged a little and homogenized at 1033 K for 86.4 k sec under an argon atmosphere, and then quenched into iced brine.

Test-pieces for hardness tests were cold-rolled into 3 mm × 7 mm × 3 mm billets. The measurements were made on test-pieces after various temperatures and periods of ageing, using a 500 g load and a diamond pyramid indentor. Discs 3 mm in diameter punched from strips that had been cold-rolled to a thickness of 0.1 mm were electrothinned by a double-jet technique for examination by TEM after being subject to the required heat treatment. The electrolyte used for this thinning was prepared by dissolving 35 g of chromium trioxide in a solution of 200 ml of acetic acid and 10 ml of distilled water. A 200 kV electron microscope equipped with a specimen tilting device was employed in the present study. Powder specimens for X-ray diffraction study were vacuum-sealed in a silica tube and subjected to heat-treatment at required temperatures and periods.

3. Results

3.1. Age-hardening characteristics

Fig. 1 demonstrates the variation of hardness during isothermal ageing at several constant temperatures. The age-hardening behaviours show a different tendency above and below 675 K; this temperature corresponds to the critical temperature of Cu_3Au ordering [5]. Below this temperature, the age-hardening curves exhibit a two-stage hardening, i.e. the curves start to increase rapidly in hardness at the initial stage

0022–2461/88 $03.00 + .12

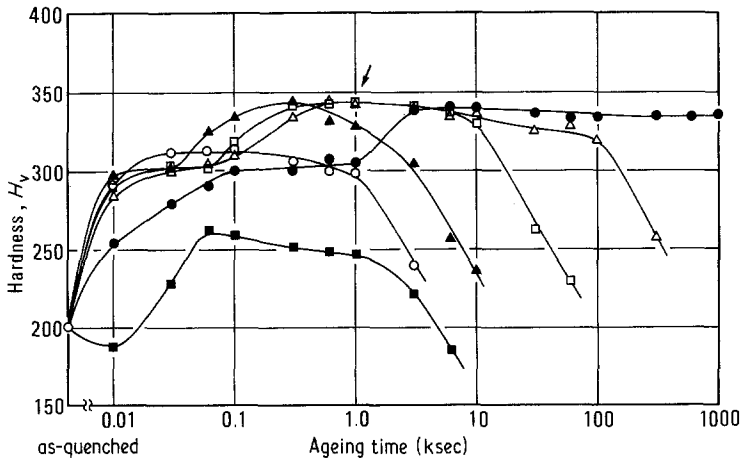

Figure 1 Isothermal age-hardening curves of the alloy solution-treated at 1033 K: (●) 573 K, (△) 613 K, (□) 633 K, (▲) 673 K, (○) 693 K, (■) 773 K.

of ageing, go through a slight stagnation of hardening, and then rise to maximum hardness.

On the other hand, above this temperature, the hardening curves show a single peak of hardness, and then maintain a relatively higher hardness during ageing. A marked softening is observed in the hardening curves after lengthy ageing periods over the whole range of ageing temperature examined in the present study. However, there is found to be a distinguishable difference in the hardening curves between 773 K and 693 K. The former shows a characteristic sigmoidal shape which implies a nucleation and growth process, even though a slight decrease in hardness is observed in the early stage of ageing. It is assumed that this softening is due to the relief of internal stress which is generated during quenching. In contrast, the hardening curve at 693 K suggests a simple growth process.

Thus, it was found that there are three distinguishable age-hardening characteristics depending on temperature in the present alloy.

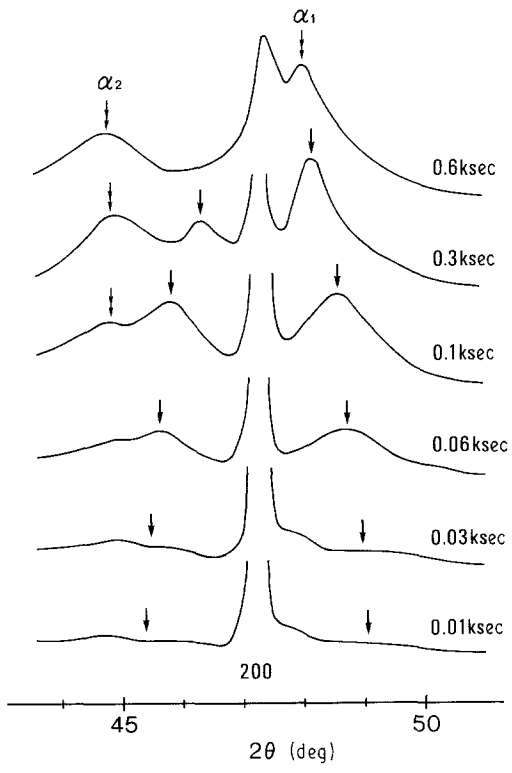

Figure 2 Changes in X-ray diffraction profile of the 200 reflection during isothermal ageing at 613 K for various periods.

3.2. Ageing below 673 K

Fig. 2 represents changes in the X-ray diffraction profile around the 200 diffraction reflection during ageing at 613 K for various periods. In the figure, double arrows indicate the α_1 and α_2 phases which are the copper-rich and silver-rich phases, respectively [5]. These phases were also observed in the X-ray diffraction pattern of the specimen quenched from 1033 K. In the present alloy, these phases formed during quenching are thought to appear unavoidably due to the misibility gap which approaches closely to the solidus plane at the composition of the present alloy, because it is difficult to obtain a single phase of solid solution by any rapid quenching method. They did not seem, however, to have a serious influence upon the analysis of diffraction patterns in the present study. On the other hand, arrows exhibit the positions of side-bands. With the progress of ageing the side-bands move closer to the main reflection. These changes suggest the formation of a modulated structure resulting from spinodal decomposition, as was observed in the 14 carat gold–copper–silver ternary alloy [3, 4].

TEM observation and SAED studies were made in order to elucidate the structural features induced by spinodal decomposition. The existence of the modulated structure is visible in bright-field images shown in Fig. 3, which are taken from specimens aged isothermally at 613 K for various periods. The modulation occurs along $\langle 1\,0\,0\rangle_{fcc}$ directions. The effect of ageing at 613 K on the modulated structure is also seen in Fig. 3, in which the averaged wavelength of the modulation increases during ageing: it is approximately 6.7 and 13.7 nm in the specimens aged for 0.06 and 30 k sec, respectively. Such a characteristic modulated structure is visible in bright-field images during the early stage of ageing below 673 K. Thus, the initial increase in hardness in this temperature range is associated with the modulated structure.

Fig. 4 shows TEM images and an SAED pattern taken from the second hardness peak as indicated by an arrow in Fig. 1. In the SAED pattern shown in Fig. 4c, superlattice reflections are found at the positions of the 100, 110 and equivalent positions though their intensity is extremely weak. This suggests the formation of an $L1_2$-type superlattice of the Cu_3Au phase by ageing in this temperature range.

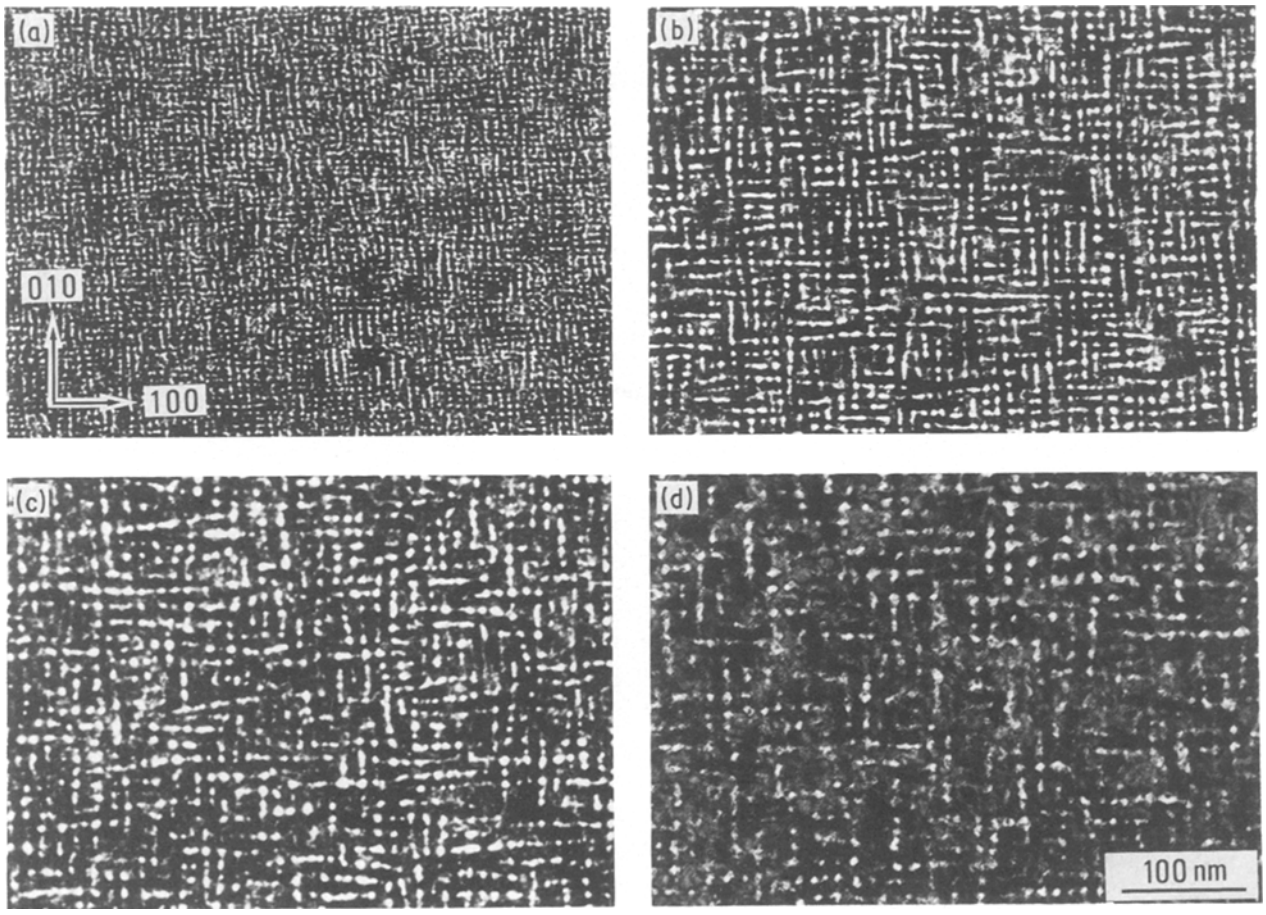

Figure 3 Effect of ageing period at 613 K on microstructure by TEM bright field image: (a) 0.06 ksec, (b) 0.3 ksec, (c) 1.0 ksec and (d) 30 ksec.

These superlattice reflections were not found in any SAED patterns taken from specimens in the early stage of ageing. Fig. 4b represents the dark-field image produced by using the 1 1 0 superlattice reflection. Bright regions of fine scale are identified as Cu_3Au ordered phase by reference to the SAED pattern of Fig. 4c and to our previous study [5]. It is thought that these fine-scale ordered regions contribute to the hardening as will be shown later.

3.3. Ageing at 693 K

Figs 5a and b show the TEM image and SAED pattern, respectively, taken from a specimen aged at 693 K for 0.01 k sec. It is seen that dense bright bands lie in a cross-hatched pattern making traces parallel to the $\langle 1\,0\,0 \rangle$ directions, as observed in Fig. 3. By prolonged ageing at 693 K these fine, bright bands grow in width and in length as seen in Figs 5c and d, which are taken from the specimen aged for 0.1 k sec. Their appearance shows without doubt the modulated structure resulting from spinodal decomposition. The microstructure varies from the fine crossed-hatched pattern to a coarser type of modulation retaining the same directionality as the cross-hatched pattern during ageing at 693 K. Furthmore, no superlattice reflections could be found in X-ray and SAED patterns obtained from this ageing temperature range. Thus, age-hardening in this temperature range is solely due to the formation of modulated structure resulting from spinodal decomposition. By further ageing, the coarser type of modulated structure was replaced by a lamellar structure growing from grain boundaries. This leads to a loss of the internal strain generated by the modulation and to a reduction in hardness.

3.4. Ageing at 773 K

Fig. 6 represents changes in the X-ray diffraction profiles during isothermal ageing at 773 K for various periods. Although the diffraction peaks shown in this figure represent only the 1 1 1 and 2 0 0 reflections, the specimen which is solution-treated, designated as α_0, gives an X-ray diffraction pattern typical of the face-centred cubic lattice. Furthermore, in spite of the fact that the α_1 and α_2 phases appear unavoidably by quenching in the X-ray diffraction pattern as seen in the bottom trace of Fig. 6, the lattice parameter is found to be $a = 0.385$ nm for the α_0 phase.

An initial change in the diffraction pattern during ageing is the appearance of two sets of diffraction peaks for the f c c lattices accompanied by shifts and changes in height of the peaks. After ageing at 773 K for 0.1 k sec, these peaks (designated as α_1 and α_2) are clearly visible in the line profile as seen at the top of Fig. 6. No superlattice reflections and/or side bands can be found at the positions expected in the X-ray diffraction patterns for various periods of ageing in this temperature. The lattice parameters of the α_1 and α_2 phases were determined as 0.380 and 0.406 nm, respectively. These changes in the X-ray diffraction patterns indicate the occurrence of two-phase decomposition by a homogeneous mechanism during ageing in this temperature range.

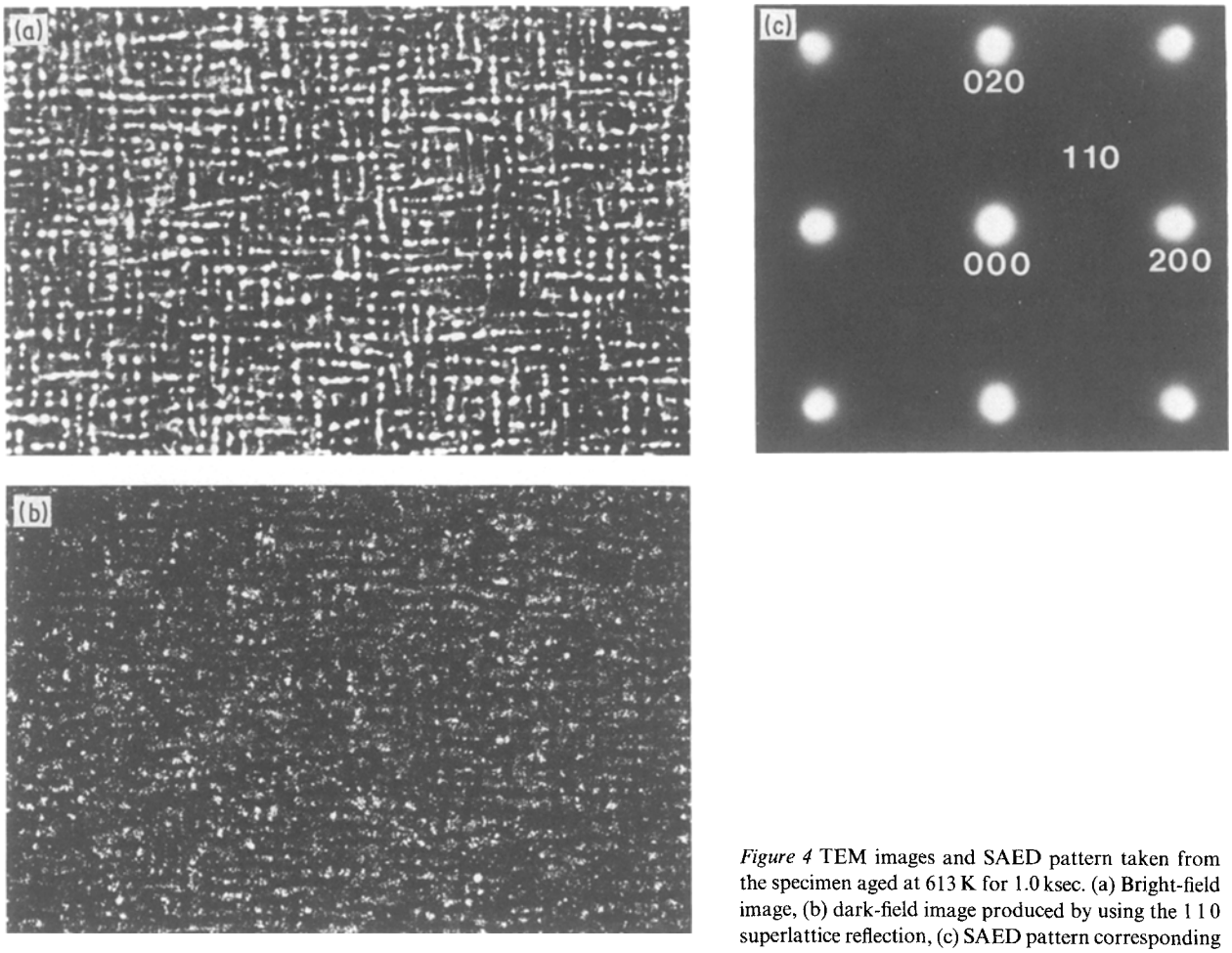

Figure 4 TEM images and SAED pattern taken from the specimen aged at 613 K for 1.0 ksec. (a) Bright-field image, (b) dark-field image produced by using the 1 1 0 superlattice reflection, (c) SAED pattern corresponding to (a) and (b).

A typical bright-field electron micrograph for this stage is given in Fig. 7, which is taken from a specimen aged at 773 K for 0.1 k sec. A number of precipitates are observed as bright bands parallel to the $\langle 1\,0\,0 \rangle$ directions in the matrix. Judging from the coherent phase diagram of the $Au_x(Ag_{0.24}Cu_{0.76})_{1-x}$ section of the ternary gold–copper–silver system [5], these precipitates are identified as the α_2 phase (silver-rich solid solution) which has an f c c structure as indicated by the SAED pattern shown as an inset of Fig. 7. The SAED pattern and TEM micrograph also indicate that the two-phase decomposition produced periodically spaced plates of the α_2 phase parallel to $\{1\,0\,0\}$ planes of the α_1 matrix. Consequently, it is thought that the plate-shaped α_2 precipitates are formed by a nucleation and growth mechanism during ageing in this temperature range.

3.5. Over-ageing and long-period superstructure of Cu_3Au

As seen in Fig. 1, a drastic reduction in hardness was observed in the age-hardening curves for prolonged ageing period over the whole range of temperature. This softening, i.e. over-ageing, coincided with the appearance of a lamellar structure from grain boundaries by a heterogeneous mechanism.

Fig. 8 shows a typical lamellar structure taken from the specimen aged at 633 K for 600 k sec. Alternating lamellae have smooth interfaces and no strain contrast as seen in Fig. 8a which is a bright-field electron micrograph. Figs 8b and c are the dark-field image produced by using the 1 1 0 superlattice reflection and the SAED pattern, respectively. The SAED pattern indicates that these alternating lamellae consist of the copper-rich α_1 phase and silver-rich α_2 phase. Because this ageing temperature of 633 K is below the critical temperature for Cu_3Au ordering, 675 K, superlattice reflections are seen in the diffraction pattern at the 1 0 0, 1 1 0 and equivalent positions of the α_1 phase. Furthermore, the 1 0 0-type superlattice reflections split into three spots, while the 1 1 0-type superlattice reflections split into five spots and form cross-like spots. These splitting of superlattice reflections suggest the formation of a periodic antiphase domain structure which resembles the AuCu(II) long-period superstructure [3, 4, 6–8]. Fig. 8b indeed shows the Cu_3Au(II) periodic antiphase domain boundaries which are positioned in two perpendicular directions. In this micrograph, it is also found that the Cu_3Au(II) ordered phase coexists adjoining the Cu_3Au(I) ordered phase, as indicated by the splitting configuration of the superlattice reflections in the SAED pattern (Fig. 8c). It should be noted that the Cu_3Au(II) ordered phase is found only in the grain boundary product.

An X-ray diffraction study was performed to confirm the stable temperature range of the Cu_3Au(II) ordered phase. Fig. 9 shows changes in the diffraction profile of the 1 0 0 and 1 1 0 superlattice reflections during ageing at various temperatures and periods.

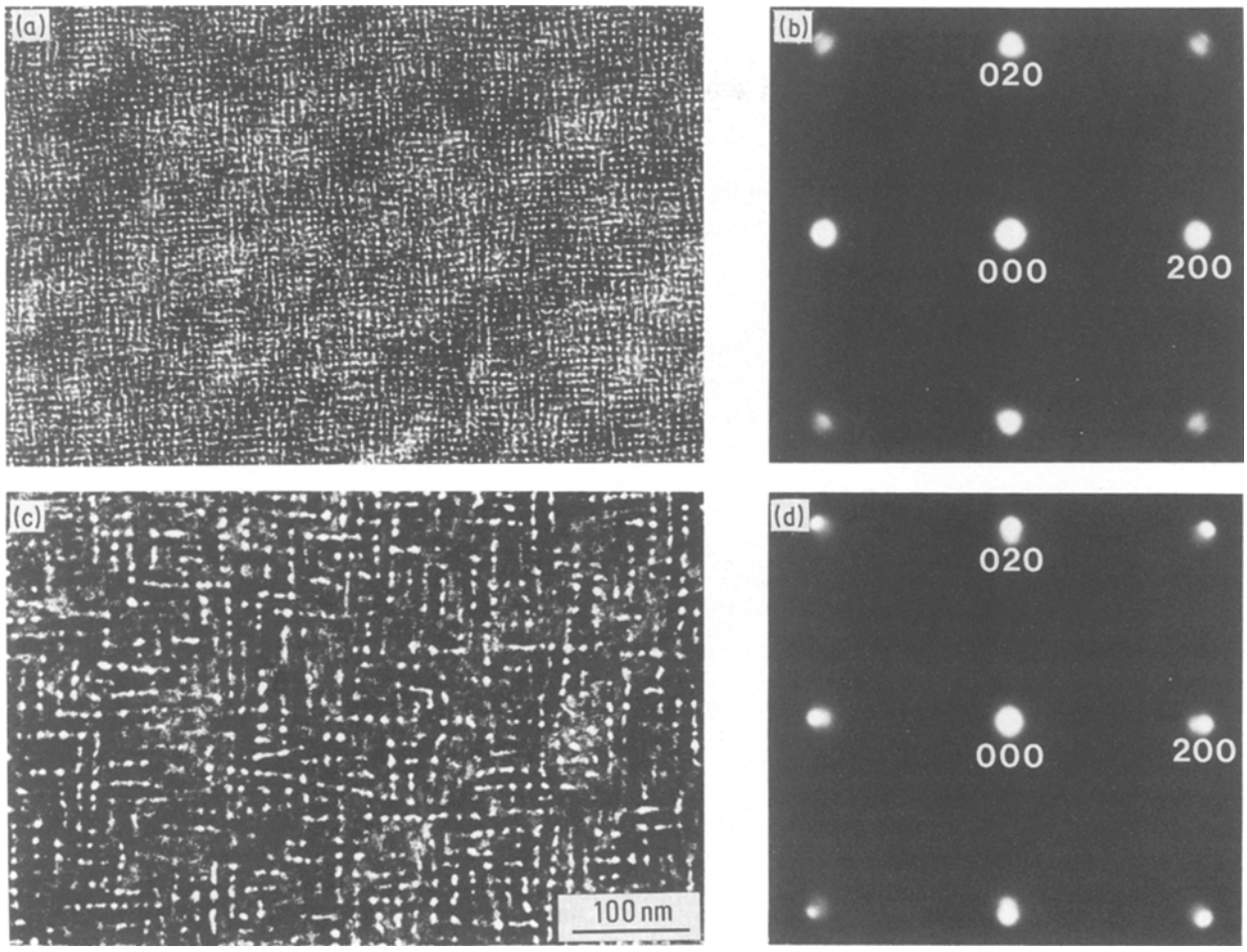

Figure 5 Effect of ageing period at 693 K on microstructure by TEM images, (a) Bright-field image taken from the specimen aged for 0.01 ksec, (b) SAED pattern corresponding to (a), (c) bright-field image taken from the specimen aged for 0.1 ksec, (d) SAED pattern corresponding to (c).

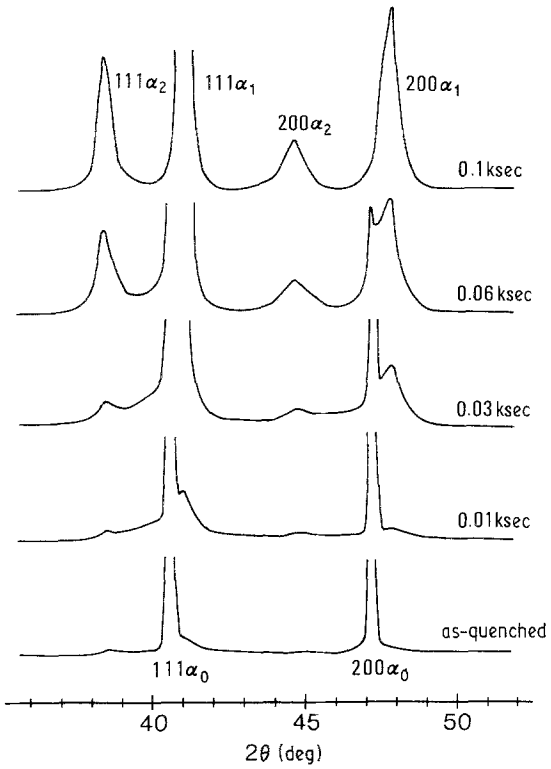

Figure 6 Changes in the X-ray diffraction profile of the 1 1 1 and 2 0 0 reflections during isothermal ageing at 773 K for various periods.

Notwithstanding the fact that splitting of the 1 0 0 superlattice reflection is impossible to find at any ageing temperature, the 1 1 0 superlattice reflection obviously exhibits side-maxima in the diffraction profiles of 633 and 628 K, as indicated by arrows. However, a shoulder appears on both sides of the 1 1 0 superlattice reflection after ageing at 623 K. This shoulder probably turns into the side-maxima on prolonged ageing. Although there is observed to be no splitting in the 1 0 0 superlattice reflection, X-ray and TEM studies demonstrate the introduction of the long-period antiphase domain structure of Cu_3Au(II) phase by ageing at temperatures between 623 and 633 K.

4. Discussion

The present results showed three distinct age-hardening behaviours depending on temperature, i.e. (i) a two-stage hardening by ageing below 673 K, (ii) a drastic hardening in the early stage of ageing at 693 K, and (iii) a characteristic sigmoidal-shaped hardening during ageing at 773 K.

By ageing below 673 K, X-ray and TEM studies revealed the following sequence of phase transformation: appearance of the modulated structure resulting from spinodal decomposition in the early stage, and then the occurrence of Cu_3Au ordering (Figs 2, 3

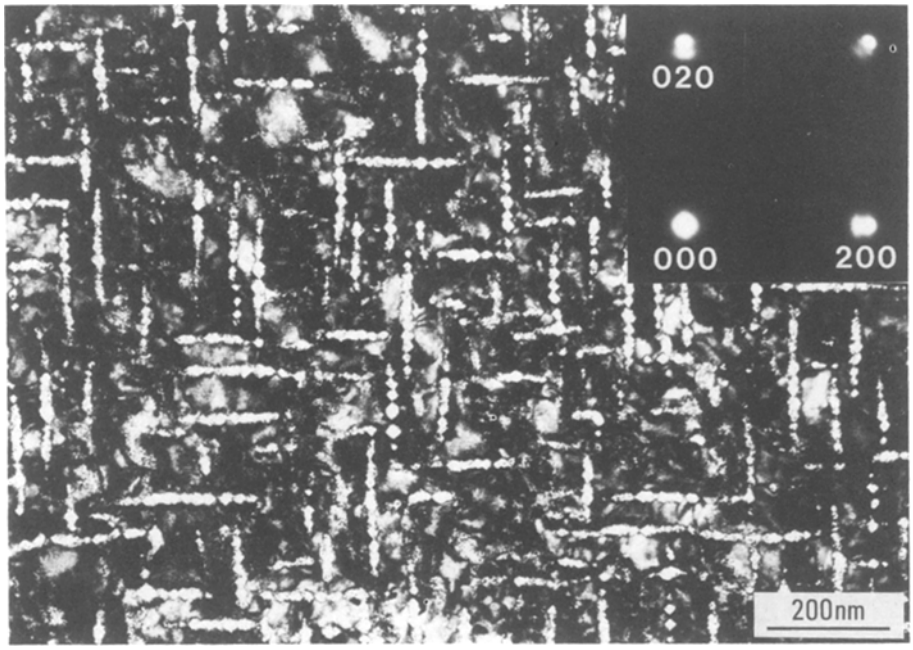

Figure 7 Bright-field image taken from the specimen aged at 773 K for 0.1 ksec and its SAED pattern (inset).

and 4). On the other hand, the age-hardening behaviour at 693 K was driven from a single process characterized by the formation of modulated structure as seen in Fig. 5, because it was assumed that this ageing temperature was above the critical temperature for Cu_3Au ordering (675 K) in the present alloy [5]. The initial increase in hardness in this temperature range, below 693 K, is apparently associated with the modulated structure. Saito and Watanabe [9] and Butler and Thomas [10] have explained that the strengthening associated with modulated structure comes from internal strain-hardening, since the formation of a modulated structure gives rise to an elastic strain field corresponding to the wavelength of modulation. Actually, strain contrast was observed in the TEM micrographs in addition to the diffuse scattering around the fundamental reflections in SAED patterns.

By prolonged ageing at 613 K, for example, the wavelength of the modulation increased from the value of 6.7 nm for 0.06 ksec to 13.7 nm for 30 ksec and

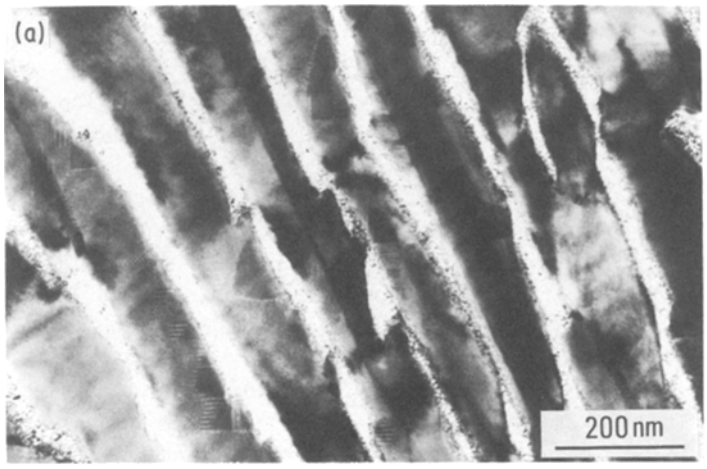

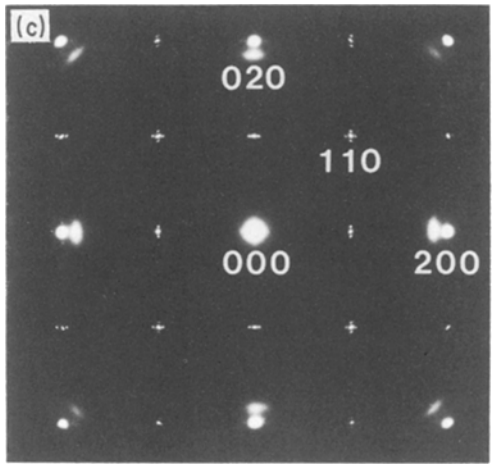

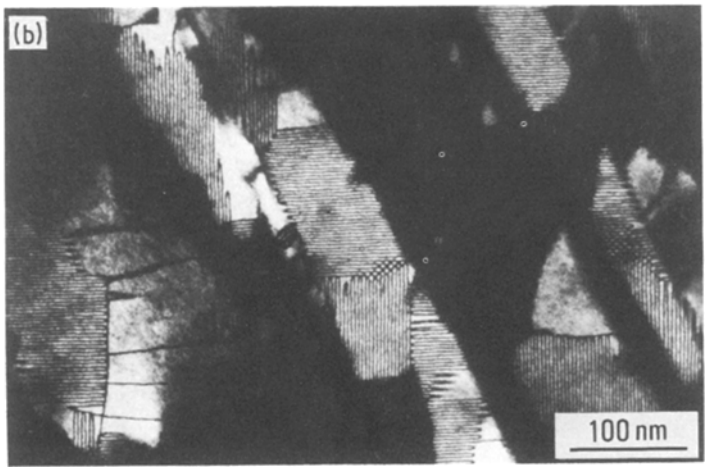

Figure 8 TEM images and SAED pattern taken from the specimen aged at 633 K for 600 ksec. (a) Bright-field image, (b) dark-field image produced by using the 1 1 0 superlattice reflection, (c) SAED pattern.

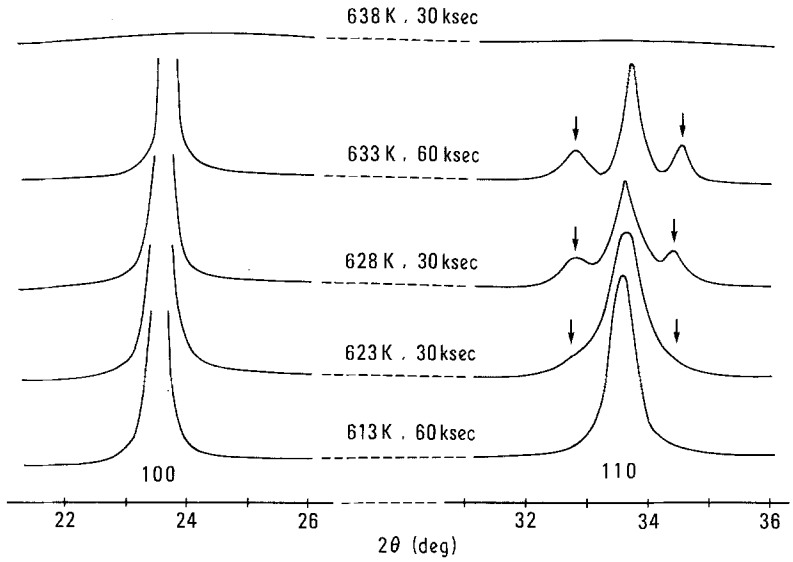

Figure 9 Changes in X-ray diffraction profile of the 1 0 0 and 1 1 0 superlattice reflections for various temperatures and periods of ageing.

a coarser-type of modulated structure was formed in the grain interior. The increase in wavelength of the modulation will gives rise to a precipitate by interpenetration of the dislocation network at the {1 0 0} interfaces between one enriched region and the other depleted region, in one component, since the elastic energy is minimum for <1 0 0> directions in most cubic systems [11]. Thus, the elastic strain fields which contribute to the hardening are accommodated at the interface between the precipitate and matrix. However, the present result showed that a considerably higher hardness was maintained for relatively prolonged ageing periods as seen in Fig. 1. Consequently, the internal strains associated with the modulation may not be relieved fully by the dislocation network at the interface until the modulated structure becomes considerably coarser.

By ageing below 673 K, the second stage of hardening was observed to be due to the Cu_3Au ordering. The hardness in the second stage increased from the initial value of 300 VHN to a maximum of 345 VHN by ageing at 673 K as seen in Fig. 1. Fine particles of the Cu_3Au ordered phase were found in the dark-field micrograph shown in Fig. 4b, which corresponded to the second hardness peak. The average particle size was measured to be $\simeq 3$ nm. Biggs and Broom [12] and Ardley [13] demonstrated that the maximum yield stress occurred at an antiphase domain size of 3 to 4 nm during isothermal ordering of Cu_3Au. On the other hand, David and Stoloff [14] concluded that the increase in strength was not due solely to a domain size effect, but to a combination of short-range order strengthening. They also stated that strengthening was generated when an antiphase boundary was induced by ageing. Fig. 4b shows that the Cu_3Au ordered particle size is too small to determine whether the antiphase domain boundary is induced or not. However, the second stage of hardening is certainly affected by the formation of fine Cu_3Au ordered particles.

Although the spinodal temperature has not been determined in the present alloy, the ageing temperature of 773 K is undoubtedly above the spinodal temperature as well as the critical temperture for Cu_3Au ordering; therfore the two-phase decomposition will be generated by a nucleation and growth mechanism during ageing in this temperature range. Actually, the changes in X-ray diffraction patterns indicated that the silver-rich α_2 phase was formed by a continuous mechanism during ageing, as seen in Fig. 6. In Fig. 7, the TEM micrograph showed the formation of plate-shaped α_2 precipitates parallel to the $\langle 1\,0\,0\rangle$ directions in the matrix by a nucleation and growth mechanism during ageing. In this situation, the lattice misfit, δ, between the α_2 precipitate and α_1 matrix is given by

$$\delta = 2\frac{d_1 - d_2}{d_1 + d_2} \simeq \frac{d_1 - d_2}{d_1}$$

if $d_1 \simeq d_2$ [15]. The lattice misfit along the $[1\,0\,0]_{\text{matrix}}$ direction is calculated from the above formula to be $+0.066$ for the specimen aged at 773 K for 0.1 ksec which almost corresponds to the hardness peak. This lattice misfit value is somewhat larger than that of the lattice misfit value, -0.045, along the [0 0 1] direction of the AuCuI superlattice, i.e. the c axis. Such an amount of lattice misfit will cause a coherent strain at the interface between the precipitate and matrix, even though the strain at the interface may be accommodated partially by the introduction of interface dislocations. Consequently, these coherent strains make a major contribution to age-hardening in this temperature range.

A marked decrease in hardness was observed coincidently with the appearance of lamellar structure at the grain boundary by lengthy ageing over the whole range of temperature. These lamellae are able to continue growing at the expense of the coarser type of modulated structure which contributes partially to hardening in the grain interior. Thus, the strain field at the interface is relieved as a result of the growth of the lamellar structure, as is found in gold–copper–silver ternary alloys [2, 4] and gold–copper–silver–palladium alloys [16].

The periodic antiphase domain structure of the Cu_3Au(II) ordered phase was only found in the copper-rich α_1 phase which consisted of lamellar structure grown from a grain boundary. Such long-period

superstructure of the Cu_3Au(II) phase was formed in the limited temperature range between 623 and 633 K. It was also found that the long-period antiphase domain size varied during isothermal ageing. The detailed results will be published elsewhere.

5. Conclusions

The following conclusions have been reached regarding the age-hardening and associated phase transformations in Au–55.2 at % Cu–17.4 at % Ag alloy.

1. Three distinguishable age-hardening characteristics depending on ageing temperature were found, i.e. (i) a two-stage hardening characterized by the appearance of a modulated structure at the initial stage and then the occurrence of Cu_3Au ordering below 673 K ageing; (ii) a drastic hardening attributed solely to the modulated structure resulting from spinodal decomposition; and (iii) a sigmoidal-shaped hardening by a nucleation and growth mechanism of silver-rich precipitate during ageing at 773 K.

2. A marked over-ageing was observed by lengthy ageing over the whole range of temperature. The over-ageing coincided with the appearance of a lamellar structure growing from grain boundaries.

3. The long-period antiphase domain structure of Cu_3Au(II) was found only in the grain boundary product formed by ageing between 623 and 633 K.

Acknowledgements

The author acknowledge with gratitude financial support from the Ministry of Education, Science and Culture, Japan by a Grant-in-Aid for Encouragement of Young Scientists (62 771 615) and a Grant-in-Aid for Scientific Research (62 570 880).

References

1. Y. KANZAWA, K. YASUDA and H. METAHI, *J. Less-Common Metals* **43** (1975) 121.
2. K. YASUDA, H. METAHI and Y. KANZAWA, *ibid.* **60** (1978) 65.
3. K. YASUDA and M. OHTA, in Proceeding of 3rd Conference on Precious Metals, Chicago, May 1979, edited by M. E. Browning (International Precious Metals Institute, New York, 1979) p. 137.
4. *Idem, J. Dent. Res.* **61** (1982) 473.
5. M. NAKAGAWA and K. YASUDA, *J. Less-Common Metals* **138** (1988) 95.
6. S. OGAWA and D. WATANABE, *J. Phys. Soc. Jpn* **9** (1954) 475.
7. D. W. PASHLEY and A. E. B. PRESLAND, *J. Inst. Met.* **87** (1959) 419.
8. A. B. GLOSSOP and D. W. PASHLEY, *Proc. R. Soc.* **A250** (1959) 132.
9. K. SAITO and R. WATANABE, *J. Phys. Soc. Jpn* **22** (1967) 681.
10. P. BUTLER and G. THOMAS, *Acta Metall.* **18** (1970) 347.
11. J. W. CAHN, *ibid.* **10** (1962) 179.
12. W. D. BIGGS and T. BROOM, *Phil. Mag.* **45** (1954) 246.
13. G. W. ARDLEY, *Acta Metall.* **3** (1955) 525.
14. R. G. DAVIES and N. S. STOLOFF, *ibid.* **11** (1963) 1347.
15. P. B. HIRSCH, A. HOWIE, R. B. NICHOLSON, D. W. PASHLEY and M. J. WHELAN, "Electron Microscopy of Thin Crystals" (Butterworth, London, 1971) p. 343.
16. K. UDOH, K. HISATSUNE, K. YASUDA and M. OHTA, *Dent. Mater. J.* **3** (1984) 253.

Received 14 September
and accepted 10 December 1987